

Production cross sections of neutron rich isotopes from a ^{82}Se beam

O. B. Tarasov¹, D. J. Morrissey^{1,2}, A. M. Amthor³, L. Bandura³,
 T. Baumann¹, D. Bazin¹, J. S. Berryman¹, G. Chubarian⁴,
 N. Fukuda⁵, A. Gade^{1,6}, T. N. Ginter¹, M. Hausmann³, N. Inabe⁵,
 T. Kubo⁵, J. Pereira¹, M. Portillo³, B. M. Sherrill^{1,6}, A. Stolz^{1,6},
 C. Sumithrarachchi¹, M. Thoennessen^{1,6}, D. Weisshaar¹

¹ National Superconducting Cyclotron Laboratory, Michigan State University, East Lansing, MI 48824, USA

² Department of Chemistry, Michigan State University, East Lansing, MI 48824, USA

³ Facility for Rare Isotope Beams, Michigan State University, East Lansing, MI 48824, USA

⁴ Cyclotron Institute, Texas A&M University, College Station, TX 77843, USA

⁵ RIKEN Nishina Center, RIKEN, Wako-shi, Saitama 351-0198, Japan

⁶ Dep. of Physics and Astronomy, Michigan State University, East Lansing, MI 48824, USA

E-mail: tarasov@nscl.msu.edu

Abstract.

Production cross sections for neutron-rich nuclei from the fragmentation of a ^{82}Se beam at 139 MeV/u were measured. The longitudinal momentum distributions of 122 neutron-rich isotopes of elements $11 \leq Z \leq 32$ were determined by varying the target thickness. Production cross sections with beryllium and tungsten targets were determined for a large number of nuclei including several isotopes first observed in this work. These are the most neutron-rich nuclides of the elements $22 \leq Z \leq 25$ (^{64}Ti , ^{67}V , ^{69}Cr , ^{72}Mn). One event was registered consistent with ^{70}Cr , and another one with ^{75}Fe . A one-body Q_g systematics is used to describe the production cross sections based on thermal evaporation from excited prefragments. The current results confirm those of our previous experiment with a ^{76}Ge beam: enhanced production cross sections for neutron-rich fragments near $Z = 20$.

1. Introduction

The discovery of new nuclei in the proximity of the neutron dripline provides a test for nuclear mass models, and hence for the understanding of the nuclear force and the creation of elements. Once neutron-rich nuclei are observed, and their cross sections for formation are understood, investigations to study the nuclei themselves, such as decay spectroscopy, can be planned. Therefore, obtaining production rates for the most exotic nuclei continues to be an important part of the experimental program at existing and future rare-isotope facilities.

A number of production mechanisms have been used to produce neutron-rich isotopes for $20 \leq Z \leq 28$ [1]. But in the last years two reaction mechanisms were the most effective at producing nuclei in this region:

- projectile fragmentation – an experiment with a ^{76}Ge (132 MeV/u) beam produced 15 new isotopes of $17 \leq Z \leq 25$ [2],

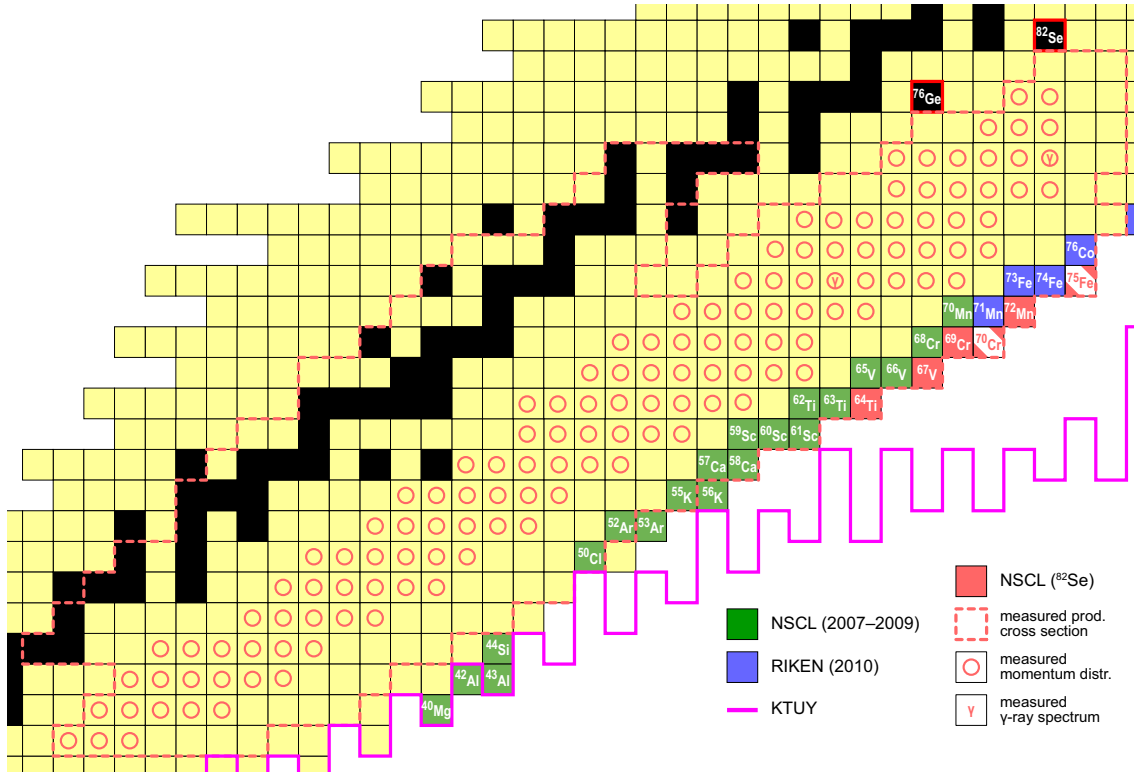


Figure 1. (Color online) The region of the nuclear chart investigated in the present work. The solid line shows the limit of bound nuclei from the KTUY mass model [7]. The new isotopes observed for the first time in the present work are marked by red squares.

- in-flight fission with light targets (Abrasion-Fission) – an experiment with a ^{238}U beam [3] produced a large number of isotopes of $25 \leq Z \leq 48$ using a Be-target, and several new isotopes with $46 \leq Z \leq 56$ by Coulomb fission on a heavy target.

Progress in the production of neutron-rich isotopes was made possible by the increase of primary beam intensities, new beam development at the National Superconducting Cyclotron Laboratory (NSCL) at Michigan State University and advances in experimental techniques [4]. Indeed, recent measurements at the NSCL [1, 4–6] have demonstrated that the fragmentation of ^{48}Ca and ^{76}Ge beams can be used to produce new isotopes in the proximity of the neutron dripline. Continuing this work, we report here the next step with a newly developed ^{82}Se beam towards the fundamental goal of defining the absolute mass limit for chemical elements in the region of calcium. In the present measurement, four neutron-rich isotopes with $42 \leq N \leq 47$ were identified for the first time (see Fig.1), one event was registered consistent with $^{70}\text{Cr}_{46}$, and another one with $^{75}\text{Fe}_{49}$.

One of the first indications of significant changes in the structure of neutron rich nuclei was the discovery of enhanced nuclear binding of heavy sodium isotopes [8]. This is now understood to result from significant contributions of *fp* shell intruder orbitals to the ground-state configurations of these isotopes [9,10]. Low-lying 2^+ states and quadrupole collectivity have been reported in neutron-rich even-even Ne and Mg isotopes around $N = 20$, see for example Refs. [11–15]. This region around ^{31}Na , where the neutron *fp* shell contributes significantly to the ground-state structure, is now known as the “Island of Inversion”. Similarly, there is mounting evidence for an onset of deformation around neutron number $N = 40$ in Fe and Cr

nuclei. In even-even Fe and Cr nuclei, for example, this evidence is based on the energies of low-lying states [16–20], transition strengths [21], and deformation length [19]. Neutron $g_{9/2}$ and $d_{5/3}$ configurations from above the $N = 40$ shell gap are proposed to descend and dominate the low-lying configurations similar to the $N = 20$ Island of Inversion [22, 23].

In our previous cross section measurements in the region around ^{62}Ti (^{76}Ge primary beam) [2] we observed a systematic smooth variation of the production cross sections that might point to nuclear structure effects, for example, an onset of collectivity, that are not included in global mass models that form the basis of systematics. The present work, since using a different primary beam, provides an independent check of this interpretation.

2. Experiment

2.1. Setup

A newly developed 139 MeV/u ^{82}Se beam with an intensity of 35 pA, accelerated by the coupled cyclotrons at the NSCL, was fragmented on a series of beryllium targets and a tungsten target, each placed at the object position of the A1900 fragment separator [24]. In this work we used an identical configuration as in our previous experiment with a ^{76}Ge beam [1], where the combination of the A1900 fragment separator with the S800 analysis beam line [25] formed a two-stage separator system, that allowed a high degree of rejection of unwanted reaction products. At the end of the S800 analysis beam line, the particles of interest were stopped in a telescope of eight silicon PIN diodes ($50 \times 50 \text{ mm}^2$) with a total thickness of 8.0 mm. A 50 mm thick plastic scintillator positioned behind the Si-telescope served as a veto detector against reactions in the Si-telescope and provided a measurement of the residual energy of lighter ions that were not stopped in the Si-telescope. A position sensitive parallel plate avalanche counter (PPAC) was located in front of the Si-telescope. All experimental details and a sketch of the experimental setup can be found in Ref. [1]. In this paper, we describe the details of our experimental approach and discuss the results.

2.2. Experimental runs

The present experiment consisted of four parts. Except for the last part, the present experiment planning was similar to the previous ^{76}Ge experiment [1]. During all runs, the magnetic rigidity of the last two dipoles of the analysis line was kept constant at a nominal value of 4.3 Tm while the production target thickness was varied to map the fragment momentum distributions. This approach greatly simplified the particle identification during the scans of the parallel momentum distributions.

The momentum acceptance of the A1900 fragment separator was restricted to $\Delta p/p = 0.1\%$ (first four runs with thin targets), and $\Delta p/p = 0.2\%$ (other targets) for the measurement of differential momentum distributions in the first part of the experiment. The use of different beryllium target thicknesses (9.7, 68, 138, 230, 314, 413, 513 mg/cm²) allowed coverage of the fragment momentum distributions necessary to extract production cross sections and also resulted in more isotopes in the particle identification spectrum.

For the second part of the experiment, a Kapton wedge with a thickness of 20.0 mg/cm² was used at the dispersive image of the A1900 to reject less exotic fragments with a 10 mm aperture in the focal plane while the separator was set for ^{67}Fe and ^{78}Zn ions. The goal of this setting was to confirm the particle identification by isomer tagging as described in Ref. [26] with ^{67m}Fe ($E_\gamma = 367 \text{ keV}$, $T_{1/2} = 43 \mu\text{s}$) and ^{78m}Zn ($E_\gamma = 730, 890, 908 \text{ keV}$, $T_{1/2} = 0.32 \mu\text{s}$).

In the third part of the experiment, dedicated to the search for new isotopes, five settings were used to cover the most neutron-rich isotopes with $20 \leq Z \leq 27$, as it was impossible to find a single target thickness and magnetic rigidity to produce all of the fragments of interest. Each setting was characterized by a fragment for which the separator was tuned. A search for the most exotic nuclei in each setting was carried out with Be and W targets. The settings were centered on

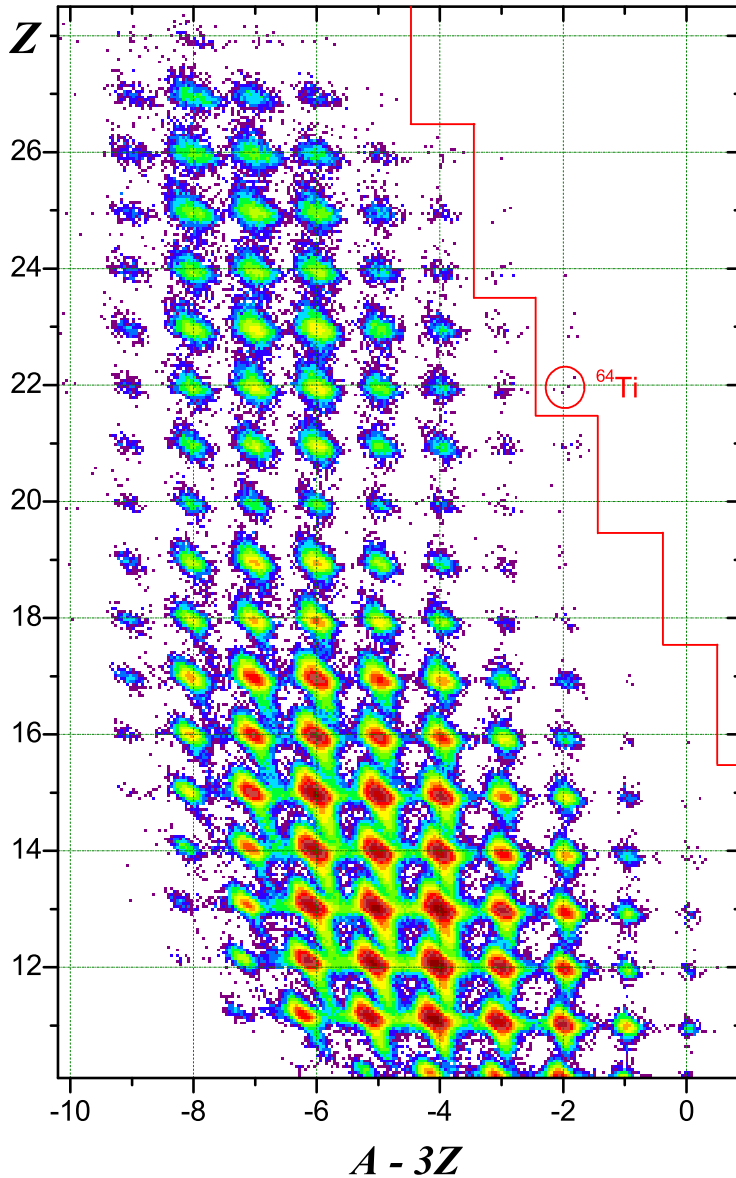


Figure 2. (Color online) Particle identification plot showing the measured atomic number, Z , versus the calculated function $A - 3Z$ for the nuclei observed in production runs of this work. See text for details. The limit of previously observed nuclei is shown by the solid red line as well as the locations of a reference nucleus (^{64}Ti).

^{60}Ca , ^{68}V and $^{74,75}\text{Fe}$ respectively, based on LISE^{++} [27] calculations using the parameterizations of the momentum distributions obtained in the first part of the experiment (see Section 3.2). The momentum acceptance of the A1900 was set to the maximum of $\Delta p/p = 5.0\%$ for these production runs. It is noteworthy that the momentum acceptance of the S800 beamline is about 4% according to LISE^{++} Monte Carlo simulations based on new extended configurations with 5-order optics. These calculations have been taken into account for the cross section analysis.

The fourth part of the experiment has been devoted to two short runs to measure the yield of more stable isotopes by centering on $^{45,48}\text{Ca}$.

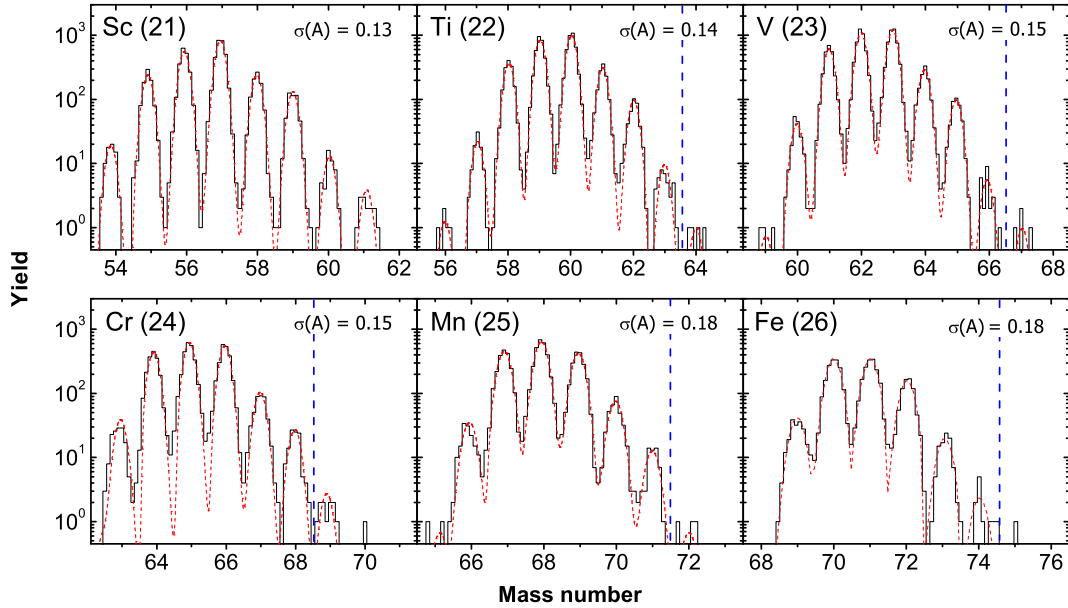


Figure 3. (Color online) Mass spectra of the elements $21 \leq Z \leq 26$. All particles that were stopped in the Si-telescope during the production runs were analyzed. The limits of previously observed nuclei are shown by the vertical dashed lines. Standard deviations produced in multi-peak fits with Gaussian distributions at constant width (dashed curves) are shown in the figures for each element.

3. Analysis of experimental data

The particle identification matrix of fully-stripped reaction products observed in the production runs is shown in Fig. 2. The range of fragments is shown as a function of the measured atomic number, Z , versus the calculated quantity $A - 3Z$. The identification of the individual isotopes in Fig. 2 was confirmed via isomer tagging using the known isomeric decays in ^{67}Fe and ^{78}Zn . The standard deviations of ionic (q) and elemental (Z) spectra were found to be similar to those in the previous experiment, therefore the probabilities of one event being misidentified as a neighboring charge state or element were as small as before. The details of the calculation of the particle identification are given in the appendix of the previous work [1].

3.1. Search for new isotopes

The mass spectra for the isotopic chains from scandium to iron measured during the production runs are shown in Fig. 3. Only nuclei that stopped in the Si telescope are included in this analysis. The observed fragments include several new isotopes that are the most neutron-rich nuclides yet observed of elements $22 \leq Z \leq 25$ (^{64}Ti , ^{67}V , ^{69}Cr , ^{72}Mn). One event was found to be consistent with ^{70}Cr , and another one with ^{75}Fe . The new neutron-rich nuclei observed in this work are those events to the right of the solid line in Fig. 2 and to the right of the vertical dashed lines in Fig. 3.

3.2. Parallel momentum distributions

The prediction of the momentum distributions of residues is important when searching for new isotopes in order to set the fragment separator at the maximum production rate. Also, the accurate prediction of the momentum distributions allows a precise estimate of the transmission

and efficient rejection of strong contaminants. In this experiment the “target scanning” approach [28] developed in the previous experiment was used to obtain parameters for the neutron-rich isotope momentum distribution models such as [29, 30]. This method is particularly well suited to survey neutron-rich nuclei since the less exotic nuclei are produced with the highest yields and their momentum distributions can be measured with the thin targets.

The data analysis of this approach has been updated, and a detailed explanation is in preparation [31]. Important improvements include: first, that the most probable velocity for a fragment is not that at the center of the target if the yield is sharply rising or falling with momentum, and second, asymmetric Gaussian distributions have been used where the asymmetry coefficients have been taken from the convolution model implemented in the LISE⁺⁺ code [27]. Note that, at the energy of these experiments, the shape of the fragment momentum distribution is slightly asymmetric with a low-energy exponential tail stemming from dissipative processes [32]. Seven targets were used to measure the momentum distributions. The momentum distributions for 122 isotopes were derived and integrated to deduce the production cross sections. A survey of all of the fitted results showed that neutron-rich fragments were produced with significantly higher velocities than the momentum distribution models [30, 33] predict, and this result is similar to our previous measurements [28].

4. Results and Discussion

4.1. Production cross section

The inclusive production cross sections for the observed fragments were calculated by correcting the measured yields for the finite momentum and angular acceptances of the separator system. A total of 122 cross sections with beryllium were obtained from the Gaussian fits to the longitudinal momentum distributions; these nuclei are indicated by stars in Fig. 4. The cross sections for all of the remaining fragments with incompletely measured longitudinal momentum distributions were obtained with estimated transmission corrections as has been done in our previous work [1]. The angular and momentum transmissions were calculated for each isotope in each setting using a model of the momentum distribution with smoothly varying parameters extracted from the measured parallel momentum distributions.

The cross sections obtained for all of the fragments observed in this experiment are shown in Fig. 4 along with the predictions of the recent EPAX 3.1 parameterization [34]. For those isotopes that relied on transmission calculations, the weighted mean of all measured yields was used to obtain the “model-based” cross section (shown by solid diamonds in Fig. 4). The uncertainties in these cases include the statistical, the systematic and the transmission uncertainties. For more details see ref. [28]. As can be seen in Fig. 4, the model-based cross sections are in good agreement with those produced by integrating the measured longitudinal momentum distributions. It is important to note that the predictions of the recent EPAX 3.1 parameterization for reactions with beryllium, shown by the solid lines in Fig. 4, reproduces the measured cross sections for isotopes much better than previous EPAX 2.15 predictions [35].

4.2. Q_g systematics

The production cross sections for the most neutron-rich projectile fragments have been previously shown to have an exponential dependance on Q_g (the difference in mass-excess of the beam particle and the observed fragment) [2, 5]. To test this behavior, the cross sections for each isotopic chain were fitted with the simple expression:

$$\sigma(Z, A) = f(Z) \exp(Q_g^*/T), \quad (1)$$

where T is an effective temperature or inverse slope. In this work neutron odd-even corrections have been applied for Q_g of neutron-odd isotopes, that do not change slopes of lines, but smooth

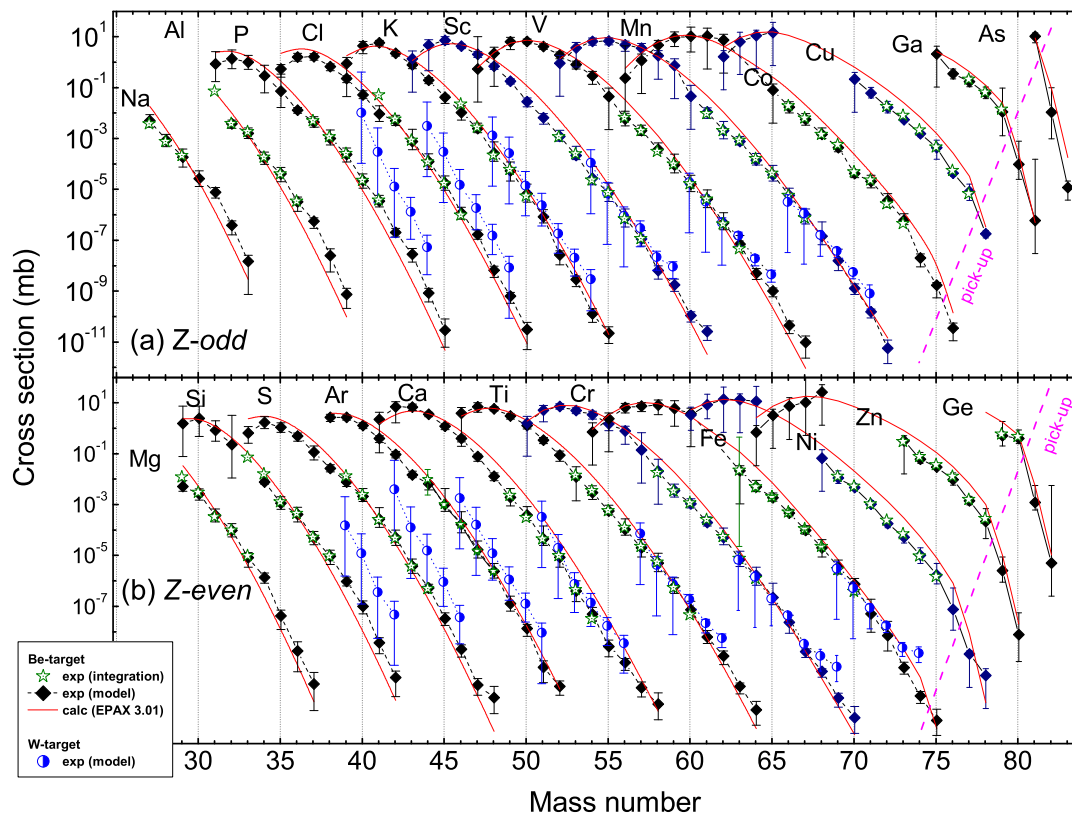


Figure 4. (Color online) Inclusive production cross sections for fragments from the reaction of ^{82}Se with beryllium and tungsten targets shown as a function of mass number. The cross sections with the beryllium targets derived by momentum distribution integration are shown by stars, those normalized with LISE^{++} transmission calculations are indicated by solid diamonds. The cross sections obtained with the tungsten target were normalized with LISE^{++} transmission calculations. The red solid lines show the predictions of the EPAX 3.1 systematics [34] for beryllium. The two magenta dashed lines separate nuclei that require neutron pickup in the production mechanism.

the data and significantly decreases the χ^2 -value. This correction has a large effect on the stable isotopes, and practically no influence for very exotic nuclei with weakly bound neutrons.

Fig. 5 represents production cross sections measured with Be targets in this experiment, where the abscissa, Q_g^* , is the smoothed difference between the mass of the ground state of the projectile and the observed fragment, where the masses were taken from Ref. [7]. As in the previous experiment, the heaviest isotopes of elements in the middle of the distribution ($Z = 19, 20, 21,$ and 22) appear to break away from the straight-line behavior. The data were fitted by two lines with a floating connection point, and results are shown by lines in the figure. The behavior of the slopes in the Q_g^* figure are summarized in Fig.6 where the two individual fitted values of the inverse slope parameter, T , for products from Be targets are shown as a function of atomic number. The corresponding plot for the W target is shown in Fig. 7. The inverse slopes of the cross sections from the previous experiment [1] with ^{76}Ge beam are shown in these figures for comparison.

Based on these figures we find that the general increase in T for all of the heavy isotopes of elements $Z = 19, 20, 21,$ and 22 observed with a ^{76}Ge beam is reproduced by this experiment

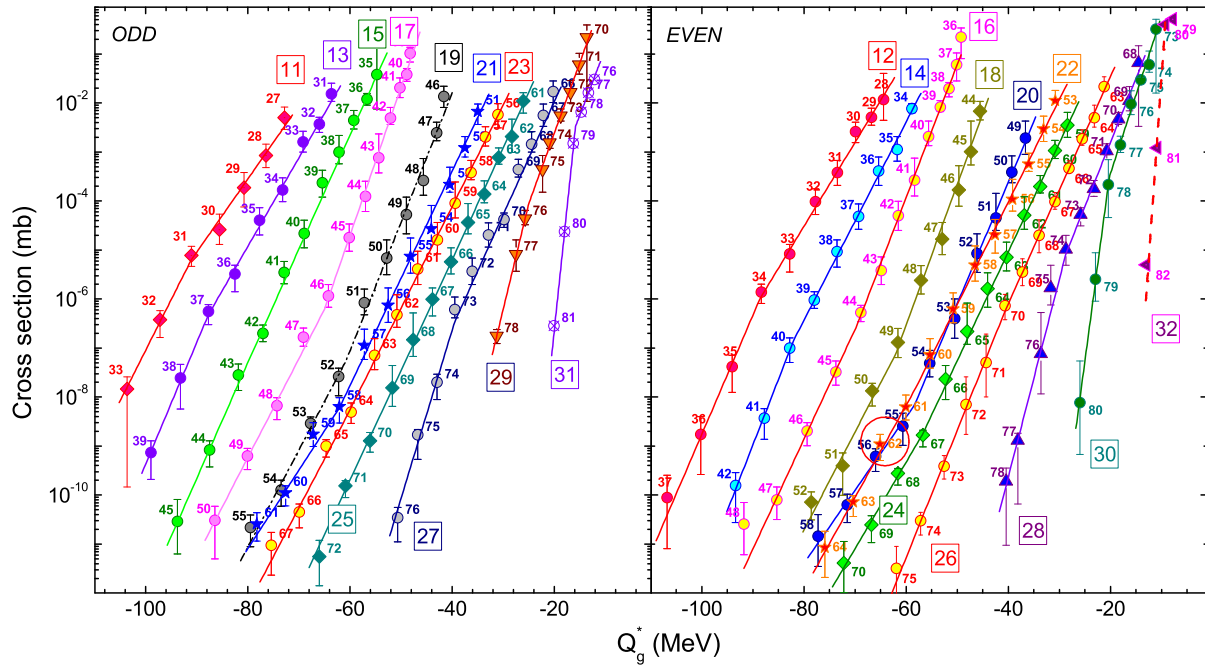


Figure 5. (Color online) Cross sections for the production of neutron-rich nuclei with odd (left plot) and even (right plot) atomic numbers, with a beryllium target. See text for explanation of Q_g^* and the lines. The cross section for ^{62}Ti at the center of the proposed new island of inversion [22] are circled.

using the ^{82}Se beam.

Small values of the inverse slope parameter T for heavy neutron-rich isotopes of elements ($Z = 27-33$) in Fig.6 can be explained by the fact that these isotopes were produced through transfer reactions (see the dashed lines in Fig. 4, which show pick-up products), and therefore the well-known Q_{gg} -systematics used for the two-body process may be more applicable.

5. Summary

The present study of the fragmentation of a ^{82}Se beam at 139 MeV/u provided evidence for the production of four previously unobserved neutron-rich isotopes. The momentum distributions and cross sections for a large number of neutron-rich nuclei produced by the ^{82}Se beam were measured by varying the target thickness in a two-stage fragment separator using a narrow momentum selection. The longitudinal momentum distributions of 122 neutron-rich isotopes of the elements with $11 \leq Z \leq 32$ were compared to models that describe the shape and centroid of fragment momentum distributions. New parameters for the semiempirical momentum distribution models [29, 30] based on the measured momenta were obtained. The most neutron-rich nuclei of elements with $Z = 19$ to 22 were produced with an enhanced rate compared to the systematics of the production cross sections from the Q_g function. This trend was previously reported for fragmentation with ^{76}Ge beam target [1].

Acknowledgments

The authors would like to acknowledge the operations staff of the NSCL for developing the intense ^{82}Se beam necessary for this study. This work was supported by the U.S. National Science Foundation under grant PHY-06-06007 and PHY-11-02511.

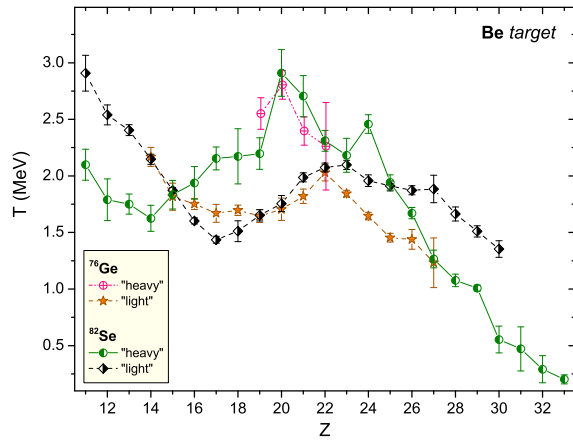


Figure 6. (Color online) Values of the inverse slope parameter, T , from the best fit of Eq. 1 to the experimental cross sections in Fig. 5 shown as a function of atomic number, where half-filled green circles for heaviest isotope and half-filled black diamonds for light isotopes produced with a ^{82}Se beam on beryllium targets, whereas open magenta circles and solid brown stars for isotopes obtained with a ^{76}Ge beam [1].

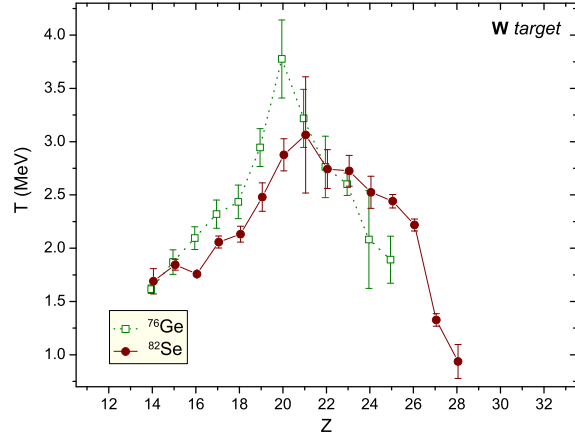


Figure 7. (Color online) Similar to Fig. 6 for data with the tungsten target.

References

- [1] Tarasov O B, Portillo M, Amthor A M, Baumann T, Bazin D, Gade A, Ginter T N, Hausmann M, Inabe N, Kubo T, Morrissey D J, Nettleton A, Pereira J, Sherrill B M, Stolz A and Thoennessen M 2009 *Phys. Rev. C* **80** 034609
- [2] Tarasov O B, Morrissey D J, Amthor A M, Baumann T, Bazin D, Gade A, Ginter T N, Hausmann M, Inabe N, Kubo T, Nettleton A, Pereira J, Portillo M, Sherrill B M, Stolz A and Thoennessen M 2009 *Phys. Rev. Lett.* **102** 142501
- [3] Ohnishi T, Kubo T, Kusaka K, Yoshida A, Yoshida K, Ohtake M, Fukuda N, Takeda H, Kameda D, Tanaka K, Inabe N, Yanagisawa Y, Gono Y, Watanabe H, Otsu H, Baba H, Ichihara T, Yamaguchi Y, Takechi M, Nishimura S, Ueno H, Yoshimi A, Sakurai H, Motobayashi T, Nakao T, Mizoi Y, Matsushita M, Ieki K, Kobayashi N, Tanaka K, Kawada Y, Tanaka N, Deguchi S, Satou Y, Kondo Y, Nakamura T, Yoshinaga K, Ishii C, Yoshii H, Miyashita Y, Uematsu N, Shiraki Y, Sumikama T, Chiba J, Ideguchi E, Saito A, Yamaguchi T, Hachiuma I, Suzuki T, Moriguchi T, Ozawa A, Ohtsubo T, Famiano M A, Geissel H, Nettleton A S, Tarasov O B, Bazin D P, Sherrill B M, Manikonda S L and Nolen J A 2010 *J. Phys. Soc. Jpn.* **79** 073201
- [4] Baumann T, Amthor A M, Bazin D, Brown B A, Folden III C M, Gade A, Ginter T N, Hausmann M, Matos M, Morrissey D J, Portillo M, Schiller A, Sherrill B M, Stolz A, Tarasov O B and Thoennessen M 2007 *Nature* **442** 1022
- [5] Tarasov O B, Baumann T, Amthor A M, Bazin D, Folden III C M, Ginter T N, Hausmann M, Matos M, Morrissey D J, Nettleton A, Portillo M, Schiller A, Sherrill B M, Stolz A and Thoennessen M 2007 *Phys. Rev. C* **75** 064613
- [6] Mantica P F, Crawford H L, Pereira J, Pinter J S, Stoker J B, Broda R, Fornal B, Janssens R V F, Wang X, Zhu S, Hoteling N, Walters W B, Hoffman C R and Tabor S L 2008 *Bull. Am. Phys. Soc.* **53** 64
- [7] Koura H, Tachibana T, Uno M and Yamada M 2005 *Prog. Theo. Phys.* **113** 305
- [8] Thibault C, Klapisch R, Rigaud C, Poskanzer A M, Prieels R, Lessard L and Reisdorf W 1975 *Phys. Rev. C* **75** 644
- [9] Campi X, Flocard H, Kerman A K and Koonin S 1975 *Nucl. Phys. A* **251** 193
- [10] Warburton E K, Becker J A and Brown B A 1990 *Phys. Rev. C* **41** 1147

- [11] Guillemaud-Mueller D, Detraz C, Langevin M, Naulin F, Saint-Simon M D, Thibault C, Touchard F and Epherre M 1984 *Nucl. Phys. A* **426** 37
- [12] Motobayashi T, Ikeda Y, Ando Y, Ieki K, Inoue M, Iwasa N, Kikuchi T, Kurokawa M, Moriya S, Ogawa S, Murakami H, Shimoura S, Yanagisawa Y, Nakamura T, Watanabe Y, Ishihara M, Teranishi T, Okuno H and Casten R F 1995 *Phys. Lett. B* **346** 9
- [13] Yoneda K, Sakurai H, Gomi T, Motobayashi T, Aoi N, Fukuda N, Futakami U, Gacsi Z, Higurashi Y, Imai N, Iwasa N, Iwasaki H, Kubo T, Kunibu M, Kurokawa M, Liu Z, Minemura T, Saito A, Serata M, Shimoura S, Takeuchi S, Watanabe Y X, Yamada K, Yanagisawa Y, Yogo K, Yoshida A and Ishihara M 2001 *Phys. Lett. B* **499** 233
- [14] Yanagisawa Y, Notani M, Sakurai H, Kunibu M, Akiyoshi H, Aoi N, Baba H, Demichi K, Fukuda N, Hasegawa H, Higurashi Y, Ishihara M, Iwasa N, Iwasaki H, Gomi T, Kanno S, Kurokawa M, Matsuyama Y U, Michimasa S, Minemura T, Mizoi T, Nakamura T, Saito A, Serata M, Shimoura S, Sugimoto T, Takeshita E, Takeuchi S, Ue K, Yamada K, Yoneda K and Motobayashi T 2003 *Phys. Lett. B* **566** 84
- [15] Church J A, Campbell C M, Dinca D C, Enders J, Gade A, Glasmacher T, Hu Z, Janssens R V F, Mueller W F, Olliver H, Perry B C, Riley L A and Yurkewicz K L 054320 *Phys. Rev. C* **72** 2005
- [16] Hannawald M, Kautzsch T, Wotr A, Walters W B, Kratz K L, Fedoseyev V N, Mishin V I, Bohmer W, Pfeiffer B, Sebastian V, Jading Y, Koster U, Lettry J, Ravn H L and the ISOLDE Collaboration 1999 *Phys. Rev. Lett.* **82** 1391
- [17] Sorlin O, Donzaud C, Nowacki F, Angeli J C, Azaiez F, Bourgeois C, Chisté V, Dlouhy Z, Grevy S, Guillemaud-Mueller D, Ibrahim F, Kratz K L, Lewitowicz M, Lukyanov S M, Mrazek J, Penionzhkevich Y E, de Oliveira Santos F, Pfeiffer B, Pougheon F, Poves A, Saint-Laurent M G and Stanoiu M 2003 *Eur. Phys. J. A* **16** 55
- [18] Adrich P, Amthor A M, Bazin D, Bowen M D, Brown B A, Campbell C M, Cook J M, Gade A, Galaviz D, Glasmacher T, McDaniel S, Miller D, Obertelli A, Shimbara Y, Siwek K P, Tostevin J A and Weisshaar D 2008 *Phys. Rev. C* **77** 054306
- [19] Aoi N, Takeshita E, Suzuki H, Takeuchi S, Ota S, Baba H, Bishop S, Fukui T, Hashimoto Y, Ong H J, Ideguchi E, Ieki K, Imai N, Ishihara M, Iwasaki H, Kanno S, Kondo Y, Kubo T, Kurita K, Kusaka K, Minemura T, Motobayashi T, Nakabayashi T, Nakamura T, Nakao T, Niikura M, Okumura T, Ohnishi T, Sakurai H, Shimoura S, Sugo R, Suzuki D, Suzuki M K, Tamaki M, Tanaka K, Togano Y and Yamada K 2009 *Phys. Rev. Lett.* **102** 012502
- [20] Gade A, Janssens R V F, Baugher T, Bazin D, Brown B A, Carpenter M P, Chiara C J, Deacon A N, Freeman S J, Grinyer G F, Hoffman C R, Kay B P, Kondev F G, Lauritsen T, McDaniel S, Meierbachtol K, Ratkiewicz A, Stroberg S R, Walsh K A, Weisshaar D, Winkler R and Zhu S 2010 *Phys. Rev. C* **81** 051304
- [21] Rother W, Dewald A, Iwasaki H, Lenzi S M, Starosta K, Bazin D, Baugher T, Brown B A, Crawford H L, Fransen C, Gade A, Ginter T N, Glasmacher T, Grinyer G F, Hackstein M, Ilie G, Jolie J, McDaniel S, Miller D, Petkov P, Pissulla T, Ratkiewicz A, Ur C A, Voss P, Walsh K A, Weisshaar D and Zell K O 2011 *Phys. Rev. Lett.* **106** 022502
- [22] Brown B A 2001 *Prog. Part. Nucl. Phys.* **47** 517
- [23] Lenzi S M, Nowacki F, Poves A and Sieja K 2010 *Phys. Rev. C* **82** 054301
- [24] Morrissey D J, Sherrill B M, Steiner M, Stolz A and Wiedenhöver I 2003 *Nucl. Instrum. Meth. Phys. Res. B* **204** 90
- [25] Bazin D, Caggiano J, Sherrill B M, Yurkon J and Zeller A 2003 *Nucl. Inst. Meth. B* **204** 629
- [26] Grzywacz R, Anne R, Auger G, Bazin D, Borcea C, Borrel V, Corre J M, Dorfler T, AFomichov, Gaelels M, Guillemaud-Mueller D, Hue R, Huyse M, Janas Z, Keller H, Lewitowicz M, Lukyanov S, Mueller A C, Penionzhkevich Y, Pfitzner M, Pougheon F, Rykaczewski K, Saint-Laurent M G, Schmidt K, Schmidt-Ott W D, Sorlin O, Szerypo J, Tarasov O, Wauters J and Zylicz J 1995 *Phys. Lett. B* **355** 439
- [27] Tarasov O B and Bazin D 2008 *Nucl. Inst. Meth. B* **266** 4657
- [28] Tarasov O B, Bazin D, Baumann T, Gade A, Ginter T N, Hausmann M, Morrissey D J, Pereira J, Portillo M, Sherrill B M, Stolz A and Thoennessen M 2010 *Nucl. Inst. Meth. A* **620** 578
- [29] Goldhaber A S 1974 *Phys. Lett. B* **53** 306
- [30] Morrissey D J 1989 *Phys. Rev. C* **39** 460
- [31] Tarasov O B and et al 2012 *in preparation*
- [32] Tarasov O 2004 *Nucl. Phys. A* **734** 536
- [33] Borrel V, Guerreau D, Galin J, Gatty B, Jacquet D and Tarrago X 1983 *Z. Phys. A* **314** 191
- [34] Sümmerer K (*Preprint 1205.5436*)
- [35] Sümmerer K and Blank B 2000 *Phys. Rev. C* **61** 034607